Simulating Space Radiation-Induced Breast Tumor Incidence Using Automata

A.C. Heuskin[1,2], A.I. Osseiran[1], J. Tang[3] and S.V. Costes[1*]

[1]Life Sciences Division, Lawrence Berkeley National Laboratory, Berkeley, CA, USA

Exogen Biotechnology Inc., Berkeley, CA, USA

[2] NAmur Research Institute for Life Sciences (NARILIS), Research Center for the Physics of Matter and Radiation (PMR), University of Namur, Namur, Belgium

Running title: Automata-based space radiation risk

* To whom the correspondence should be addressed: S.V. Costes (svcostes@lbl.gov), Life Sciences Division, Lawrence Berkeley National Laboratory, 1 Cyclotron Road, MS: 977, Berkeley, CA 94720, USA. Tel: (510) 486-6988/6624, Fax: (510) 486-7542.

Abstract:

Heuskin A.C., Osseiran A., Tang J. and Costes S.V., Simulating Space Radiation-Induced Breast Tumor Incidence Using Automata, *Radiat. Res.*

Estimating cancer risk from space radiation has been an ongoing challenge for decades primarily because most epidemiological data showing evidence of cancer risk from ionizing radiation are derived from studies of atomic bomb survivors, where individuals were exposed to acute dose of gamma-rays instead of chronic exposure of high-LET cosmic radiation. In this work, we introduce a formalism using cellular automata to model the long-term effects of ionizing radiation in human breast for different radiation quality. We first validate and tune parameters for an automata-based two stage clonal expansion model which simulates the age dependence of spontaneous breast cancer incidence in unexposed US population. We then test the impact of radiation perturbation in the model by modifying parameters to reflect both targeted and non-targeted effects of ionizing radiation.

Targeted effects (TE) reflect the immediate impact of radiation on cell's DNA with classic endpoints being gene mutations and cell death. They are well known and are directly derived from experimental data. In contrast, non-targeted effects (NTE) are persistent radiation effects affecting both damaged and undamaged cells, they are non-linear with dose and they are not well characterized in the literature. TE is first introduced in the model and predictions are compared to epidemiologic data of the A-bomb cohort. TE alone is not sufficient to induce enough cancer and genomic instability which last ~100 days post-exposure independently of dose needs to be added to predict accurately the dose dependence of breast cancer induced by gamma-rays. Finally, by integrating experimental RBE for TE and keeping radiation-induced genomic instability constant with dose and LET, the model predicts that RBE for breast cancer induced by cosmic radiation would be maximum at 220 keV/µm. This work is well suited to explore next the impact of chronic low dose exposure, inter-individual variation and more complex space radiation scenarii.

1. Introduction

Space programs are currently shifting to planetary exploration, in particular missions to the moon and Mars. However, the continuous exposure of astronauts to Galactic Cosmic Rays (GCR) is one of the main concerns for long term missions because of increased risk of cancer and other degenerative diseases. The GCR spectra contains a large component of high-LET particles, such as He ions and heavier ions such as carbon and iron (HZE particles, i.e. particles with high charge and energy) (1). Despite the low frequency of GCR, they are a major contributor to cancer risk because of their high ionization density which can lead to severe mutational events. High-LET ionizing radiation have been shown to induce relative biological effectiveness (RBE) as high as 40 in animal models (2). Also of concern are solar particle events (SPE) (3) whose unpredictable nature and high doses pose a risk for out-of-spacecraft tasks.

Unfortunately, estimating cancer risk from space radiation remains a challenge primarily because most epidemiological data showing evidence of cancer risk from ionizing radiation are derived from studies of atomic bomb survivors (4). Classic risk models rely on scaling variables, such as radiation-quality factor Q, RBE and dose and dose-rate effectiveness factors, extrapolating risk from gamma radiation (main radiation in A-bomb blast) to high-LET radiation in space.

This poses the question of whether risk estimates derived from sparsely ionizing radiation can be used to assess risks associated with HZE. In this work, we introduce a formalism using cellular automata, to test mechanisms that can reproduce cancer incidence, by modeling the short-term and long-term effects of ionizing radiation in tissue. Cellular automata are stochastic models where each cell is represented by an algorithmic entity with basic individual properties representing the variety of cellular behaviors (5, 6). We first establish a relationship between the dose from gamma-radiation and cell death, cell senescence, and genomic instability for various time scale. This relationship is tuned so that

we can predict accurately breast cancer incidence in humans (A-bomb cohort vs unexposed population). In a second phase, the model is used to test new mechanisms of DNA misrepair and cell death from high-LET (7) to predict high-LET response and RBE for various cosmic radiation. This model is a first step for the growing demand of a deeper knowledge of biological processes underlying carcinogenesis and their disruption by heavy ions (1).

2. Material and methods

2.1 Multistage expansion model: theoretical considerations

We focused on the concept of the multistage expansion model which provides an analytical solution to epidemiological cancer incidence (8). This model assumes that malignant tumors arise from a series of modifications of a single progenitor cell and that cancer is the last of a series of *k* sudden and irreversible changes. For a cell which has already experienced *(i-1)* changes, the event rate for the next change is μ_i. The exact solution can be derived from Bateman's solution of successive radioactive decays and the stage $p_{m-1}(t)$ can be expressed as:

$$\boldsymbol{p_{m-1}(t) = c_m \sum_{j=1}^{m} X_{j,m} e^{-\mu_j t}} \quad (1)$$

with $c_m = \alpha \prod_{j=1}^{m-1} \mu_{j-1,j}$ and $X_{j,m} = \prod_{\substack{l=1\ldots m \\ l \neq j}} (\mu_l - \mu_j)^{-1}$. The hazard rate is then $h(t) = N\mu_k p_{k-1}(t)$ with *N* as the total number of affected cells. The first non-vanishing term in a Taylor serie of $p_{k-1}(t)$ gives the well-known Armitage-Doll model (9):

$$\boldsymbol{h(t) = a t^{k-1} \; with \; a = \frac{\prod_{j=1}^{k} \mu_j}{(k-1)!}.} \quad (2)$$

77 However this simpler model gives a power law for the age-dependent incidence and it is known that the
78 cancer incidence flattens above age 60 and falls below the predicted curve. Pompei and Wilson
79 proposed a modified version of this model by adding a senescence factor and assuming that malignant
80 cells are mortal in the sense of Hayflick (i.e. cell divisions are not infinite) (10). If a malignant cell is
81 completely senescent, this cell does not produce observable cancer. The hazard function better fits the
82 epidemiological data at high age (11) and takes the following form:

83 $$\boldsymbol{h(t) = at^{k-1}(1 - \beta t)}. \quad (3)$$

84 However not all the initiated cells can progress to cancer as some of them can be repaired or removed.
85 This lead to a more refined model involving only two stages (k=0,1,2) and a death rate for intermediate
86 cells (12, 13). The Moolgavkar, Venzon and Knudson (MVK) model or two stage clonal expansion (TSCE)
87 model gives then a hazard of the form:

88 $$\boldsymbol{h(t) = \frac{X_m(e^{(\gamma+2q)t}-1)}{q(e^{(\gamma+2q)t}+1)+\gamma}} \quad (4)$$

89 where X_m, γ and q can be related to actual biological parameters using the following transformations:

90 $X_m = \mu_2 \nu;\ \gamma = \alpha - \beta - \mu_2;\ q = \frac{\mu_2}{1-A}$ with $A = \frac{b+\sqrt{b^2-4\alpha\beta}}{2\alpha}$ and $b = \alpha + \beta + \mu_2$. Here ν is the
91 proportion of healthy cells that will acquire a first mutation, μ_2 is the rate of the second mutation, α and
92 β are growth and death or differentiation rate for intermediate cells respectively. This model can be
93 thought of as the initiation-promotion-progression paradigm of carcinogenesis.

2.2. Non exposed tissue

2.2.1. Tissue description Because deterministic models are not well suited to simulate heterogeneous tissue and as our lab is establishing a long-term computer framework for more complex radiation simulations, we use instead automata to simulate cancer incidence via the principle of TSCE. An important reason for this choice is the fact that it is easy to add new rules or different geometrical configurations in automata, making them an ideal framework for evolving simulations.

Simulations were performed using Matlab software (The MathWorks, Natick, MA, USA) and the advanced imaging platform DIPimage (Image Processing Toolbox for Matlab, Delft University of Technology, Delft, The Netherlands). The simulated tissue consists of an array of 100 X 100 pixels, with each pixel labeled with a particular stage. Fig 1A depicts conceptually the progression of a normal cell via successive mutations towards becoming a tumor cell, highlighting the importance of tissue proliferation for cancer to occur. The automata implementation of this progression is depicted in Fig. 1B with a flow chart showing decision algorithms. Stage 1 represents a normal cell (green pixel), Stage 2 (labeled in blue) is a cell harboring a potentially dangerous mutation in the context of cancer induction (i.e. initiated) and Stage 3 (red pixel) is a cell harboring the two necessary mutations to expand into a full-blown cancer. Fig. 1C shows snapshots of one simulation where tissue is progressing towards cancer over many years.

With the TSCE assumption, cell death is a necessary condition for neighboring cells to be dividing and potentially acquiring mutations. The automata approach assumes additionally that the tissue is in homeostasis which means that dead cells are rapidly replaced by newly dividing cells. Consequently, division and death rate are identical (α=β). It can be noted in Fig. 1B that all cells touching a dying cell are eligible to fill the gap that is left behind. The selection of which neighboring cell will fill the gap is drawn randomly. Thus, whenever a cell divides, the new cell filling this gap has an opportunity to

acquire a mutation related to carcinogenesis. In a general implementation of this model, if the mother cell carries *n* mutations, there is a probability that the daughter cell will carry *n+1* mutations. A cell harboring a lot of mutations is likely to be more unstable genetically. Because there is no clear law defining the relationship between progression and genomic instability, for now we are imposing a mutation rate proportional to the cell stage. This assumption allows us to reduce the number of mutation parameter to only one value: i.e. μ, the spontaneous mutation rate in a healthy cell. Note that both stage 2 and 3 can be reached via various unique combinations of genes being mutated, but details on genetic changes that lead to this pre-cancer states are not necessary in this model, as it is fully encompassed by determining μ. Mutation model can be summarized as:

$$\boldsymbol{\mu_n = n \cdot \mu}. \quad (5)$$

In this approach, division is therefore driven by the turnover of the tissue being simulated. In the case of breast, it has been shown that the cell death rate β is periodic due to the menstrual cycle of estrogen and progesterone. Rising progesterone levels drive mammary cells in ducts and alveoli to multiply for possible pregnancy. If not pregnant, progesterone levels drop and induce cell death of newly formed tissue. If we assume a 28-day cycle with an apoptotic peak between days 28 and 0, the death rate pattern for different ages can be modeled (Fig. 2A). The amplitude and average values used here are derived from the literature and they are lower with increasing age (14-16) with a rate β in the order of 10^{-3}/day/cell. At menopause, the death rate is considered flat and lower than the pre-menopause value (17). For each simulated person, the age at menopause for an *in silico* individual is established based on a triple Gaussian distribution (centers: 50.3 y.o., 42.9 y.o and 35.3 y.o.) as previously suggested (18) leading to a smooth drop of cell death in simulations as one can visualize in Fig. 2B. Note that parameters for normal cell turnover in the breast are not changed for the rest of this model since they are directly derived from the literature.

2.2.2. Senescence Senescent cells are also considered in this model. They are represented as pixels that are unable to divide nor die (i.e. Stage -1). In other words, senescent pixels no longer divide and have acquired resistance to apoptotic signals. Our senescence model takes into account the age of the tissue being simulated. Telomere-initiated cellular senescence is also included in the model by generating senescence in only dividing cells. Briefly, at each time step, a random number is generated for each stage 1 and stage 2 pixel. This number is compared to the senescence probability which changes as the square of the age of the tissue (19):

$$\boldsymbol{p_{senescence} = sen_{factor} * age^2}. \quad (6)$$

If the random number is less than $P_{senescence}$, the cell is set to stage -1. Running a parameter sweep on the senescence factor sen_{factor}, a value of $5x10^{-9}$/day led to a curve matching the literature for primates (19) (Fig 2C). In addition, a baseline of 2% senescence was imposed on the tissue at the starting age of 20 y.o. to reflect the primate data. Note that compared to primates, the age scale has been expanded to reflect the human life span. We also assumed that stage 3 pixels (cancer cells) cannot senesce anymore since they have acquired mutations that allow them to avoid telomere-dependent and oncogene-dependent senescence (20).

2.2.3. Parameter calibration to match breast cancer data Key parameters in the TSCE model are the mutation rates: i.e. initiation (with probability $\mu_1=\mu$) and transformation ($\mu_2=2\mu$). Because of our assumption about increase of genomic instability with progression, we only need to determine μ. It turns out that cancer incidence frequencies are not only dependent on μ but also on the size of the tissue being simulated. In order to understand this relationship, we performed a parameter sweep on μ for different number of cells considered in each modeled duct, and determined values of μ that led to simulations matching published spontaneous cancer incidence. Note that Age-Specific SEER Breast Cancer Incidence Rates were taken from SEER cancer registry records 2008-2012 (http://seer.cancer.gov/csr/1975_2012/) (21). Fig. 2D shows simulated cumulated cancer incidence predicted by the model for various initial tissue size being considered against SEER records (diamonds and dash-line for fit). Simulations were repeated 10 times with group of 50 *in silico* people and parameter sweep on μ was conducted to lead to the lowest mean square error between prediction and published data. We show that simulations fit very accurately epidemiologic data for various tissue size as long as the mutation rate is adjusted consequently, noting that the larger the number of cells being simulated in the tissue, the lower μ needs to be. This relationship was well behaved with a power dependence of μ over the number cells being simulated (R^2>0.999, data now shown). Ideally, one would like to simulate tissue of realistic sizes, however this would be extremely time consuming for simulations and our data suggest as long as μ is set accordingly with the tissue size, the model behaves correctly. We therefore used going forward for our radiation prediction an initial tissue size of 100x100, leading to a μ value of $3.8\text{x}10^{-6}$. Each individual was simulated as a branch of a mammary duct made of 10,000 cells (22).

Parameters having the greatest impact on the final curve are μ and β. Cell death rate β is defined by the menstrual cycle for normal cells only (stage 1), which represents the majority of the cells at the beginning of simulation (age 20) and is fixed by experimental data (Fig. 2A). On the other hand, once a

cell has become mutated, it becomes hormonal independent and cell death is only driven by genetic instability which increases with progression (see Fig. 1A). For example, high grade tumors have higher level of apoptosis and genomic instability which is usually correlated with poor prognosis (23-25). A parameter sweep was performed on the β value for stage 2 and stage 3 to best fit experimental incidence and values are summarized in Table 1, confirming β needs to increase with progression to get accurate cancer prediction.

Note that during parameter sweep, increasing either μ or β_2 and β_3 led to higher cancer incidence and thus multiple solutions for the same final cumulated incidence at age 80. However, a single solution was obtained by minimizing the error along the full age dependence between the published data and the simulations. This was done by finely tuning β_2 and β_3 down while increasing μ. Note that a cancer growth factor is also present in the model and was based on the assumption that it takes 20 years between an initiating event and a detectable cancer. The growth factor is a metric representing the ability of neoplastic cells (stage 3) to grow and expand over neighboring healthy cells. After a set number of iterations, all stage 3 cells take over their immediate neighbors. This process reflects the loss of contact inhibition in cancer cells and loss of checkpoints regulating mitosis. The tumor growth parameter was set to once a year for breast cancer and is easily tunable to model other types of more aggressive cancers and is relatively arbitrary since a cancer is scored in our model once 5% of the tissue has become stage 3.

2.2.4. Impact of senescence on cancer incidence We investigated the hypothesis that senescent cells can slow down cancer progression. The senescence response is widely recognized as a potent tumor suppressive mechanism (26-28). The senescent factor parameter was thus increased to reach various level of senescence at age 80 and the impact on cancer incidence was assessed. Our baseline level of senescence that was kept for the rest of the simulations gives around 13% senescence in the whole tissue and 11.2 ± 1.31 % incidence at age 80. Increasing the final level of senescence to 40% only reduces the incidence of breast cancer to 9.4 ± 1.27 %. The effect is more noticeable when senescence hits unrealistic values of 70% and above, leading to breast cancer incidence below 6%.

3. Results

3.1. Targeted effects

After calibrating parameters to fit spontaneous cancer incidence from epidemiological data, our model was then used to predict level of excess breast cancer one would expect from exposure to low-LET. This was done by modifying transiently mutation and cell death rates using published data in human cells exposed to low-LET.

The additional death rate from radiation was derived from clonogenic data of Lin *et al.* who studied the response of nonmalignant MCF10A mammary epithelial cells (29) and dose dependence was simulated by using the alpha/beta fit model (see Table 2). However, cells are not expected to die readily after X-ray exposure, as this is not what is observed in cell culture and even less *in vivo*. Rather the cells undergo a few cell cycles before dying either through apoptosis, necrosis or mitotic catastrophe. Mitotic catastrophe is not a cell death mechanism *per se*, but the process by which the cell will lose its reproductive capacity: i.e. following exposure to radiation, some cell lines and cancer cell lines in particular will continue to divide despite harboring DNA damage. These uncontrolled divisions lead to the loss of chromosome material, up to the point that daughter cells are no longer able to divide. The

time it takes for a cell to die was therefore modeled in two ways. First, we assume that death was spread evenly through a 14-day period based on previous work (30). For example, implementation of this model led to an additional 5.7% of all cells being deleted randomly every day for 14 days following 3 Gy X-rays (Fig. 3A – "beta const" model) before returning to the normal β value of Fig. 2A. The other death model we used assumed death rates change over time post-exposure with an exponential attenuation as suggested by *in vitro* work (31, 32). This was implemented by assuming an exponential decay over 14 days, imposing the same overall amount of death during the 14 day period following exposure. We tested two conditions: either 2 or 3 fold increased death at day 0 compared to the "beta const" model (i.e. "beta X2" model has 11% excess death at day 0 and "beta X3" model has 17% excess death at day 0 for 3 Gy exposure). Fig 3B illustrates the exponential model for "beta X3".

In the two stage clonal expansion model (TSCE), mutation rates encompass many possible genetic targets to obtain an initiated (μ_1) or transformed (μ_2) cell. To predict the impact of radiation perturbation on the TSCE we now need to propose a model affecting the mutation rate after exposure to ionizing radiation. We will assume radiation induces a transient increase of μ which is proportional to dose for 24 hours post-exposure. Let us explain why in the next paragraph.

As we and others have previously shown in great length, mutation rates are a function of radiation dose with larger genes being more likely mutated (33-35). In addition, gene location in the nucleus probably plays a role in mutation frequency since damage production and DNA repair are modulated by chromatin territories (36, 37) and therefore individual genetic predisposition are at play here. However, as a first gross approximation, one can argue that initiation and transformation mutation rates are mainly the result of point mutations or small deletions of a large and unknown DNA target and that large deletions induced by two separate DNA double strand breaks can be neglected since they often lead to cell death due to deletion of vital genes (35). This simplifies greatly the model by not requiring a

quadratic dose term and by assuming mutation rate is increased linearly with dose during exposure. The amplitude of such increase can be approximated using experimental data measuring DNA double strand break (DSB) levels in human cells. According to our previous work and literature data, baseline damage in peripheral blood lymphocytes (PBL) range from 0.004 foci/cell in children up to 0.2-1 foci/cell in healthy adult donors when measured either using the γ-H2AX assay or 53BP1 assay (38-41). Let us chose the mid-range value (0.5 foci/cell) as a baseline damage level without radiation in a healthy population. Thus, this level of endogenous damage is directly correlated to the spontaneous mutation rate μ. Next, low linear energy transfer (LET) exposure yields approximately 30 DSB/cell/Gy (42). This gives a 30/0.5 = 60 ratio for foci levels between control cells and cells irradiated by 1 Gy. This dose dependence can be generalized as followed in the TSCE model:

$$\boldsymbol{\mu(D) = 60.\mu_n.D} \quad (7)$$

where D is in Gy and μ_n is increased only for 24 hour post-exposure. Such perturbation is depicted in Fig 3C for various doses.

Radiation perturbations of μ and β parameters in the TSCE model were simulated for doses of X-rays ranging from 0.05 to 3 Gy. Note that targeted effects were entirely modeled from experimental *in vitro* data and they were integrated into the TSCE model, making our simulations true predictions and not fits. The predicted excess relative risk (ERR) was compared to breast cancer ERR in atomic bomb survivors (4). Preston *et al.* computed ERR at age 70 for individuals irradiated at age 30 following Hiroshima and Nagasaki bombardments. Our simulations were therefore stopped at age 70 to match Preston reference, and the three different death models were tested (death rate constant – "beta const", death rate decreasing exponentially – "beta 2X" and "beta 3X"). Simulations were carried out for 10 groups of 50 people. Predicted ERR shown in Fig. 3D indicate that the exponential cell death rate models predict accurately the A-bomb data for large doses (2 and 3 Gy). This is not true for lower doses,

where predictions are well below the observed ERR. In contrast, constant cell death model leads to underestimation of the reported atomic bomb data for any simulated doses, which suggests that additional mechanisms have to be taken into account to explain the observed levels of cancer. We hypothesize in this case non-targeted effects are at play, which are investigated next.

3.2. Non-targeted effects

Non-targeted effects (NTE) reflect the impact of radiation on modifying cell signaling and the tissue microenvironment following exposure to ionizing radiation which lead to systemic changes in entire organs. These have additional impacts from the classic targeted effects (i.e. direct DNA damage and cell death already simulated in the previous section). We use modeling in this section to evaluate the level of NTE required to explain the lower cancer incidence we predicted in the low dose range by only considering targeted effects (Fig 3C).

Two NTE models were tested: radiation induced genomic instability (RIGI) and radiation-induced chronic inflammation (RICI). RIGI was implemented by increasing the mutation rate in the entire tissue in a uniform manner for prolonged periods after irradiation (i.e. $\mu_{GIN} = \mu.f_{GIN}$) where μ_{GIN} is the new mutation rates in tissue when RIGI is active and f_{GIN} is the multiplicative factor induced by radiation. Let us use our model to evaluate f_{GIN} and see how it depends on dose. This can be done by doing a parameter sweep for RIGI duration and f_{GIN} leading to an array of simulated ERR. This is visualized in Fig. 4A, where predicted ERR for 3 Gy irradiation are shown as a plane. Irradiation was delivered *in silico* at age 30 and ERR assessed at age 70 to match the conditions used in the cancer breast A-bomb data (4). The intersection of the plane in Fig. 4A with the published ERR value (i.e. 2.2 at 3 Gy) represents all pair of duration and multiplicative factor f_{GIN} that can lead to the right ERR.

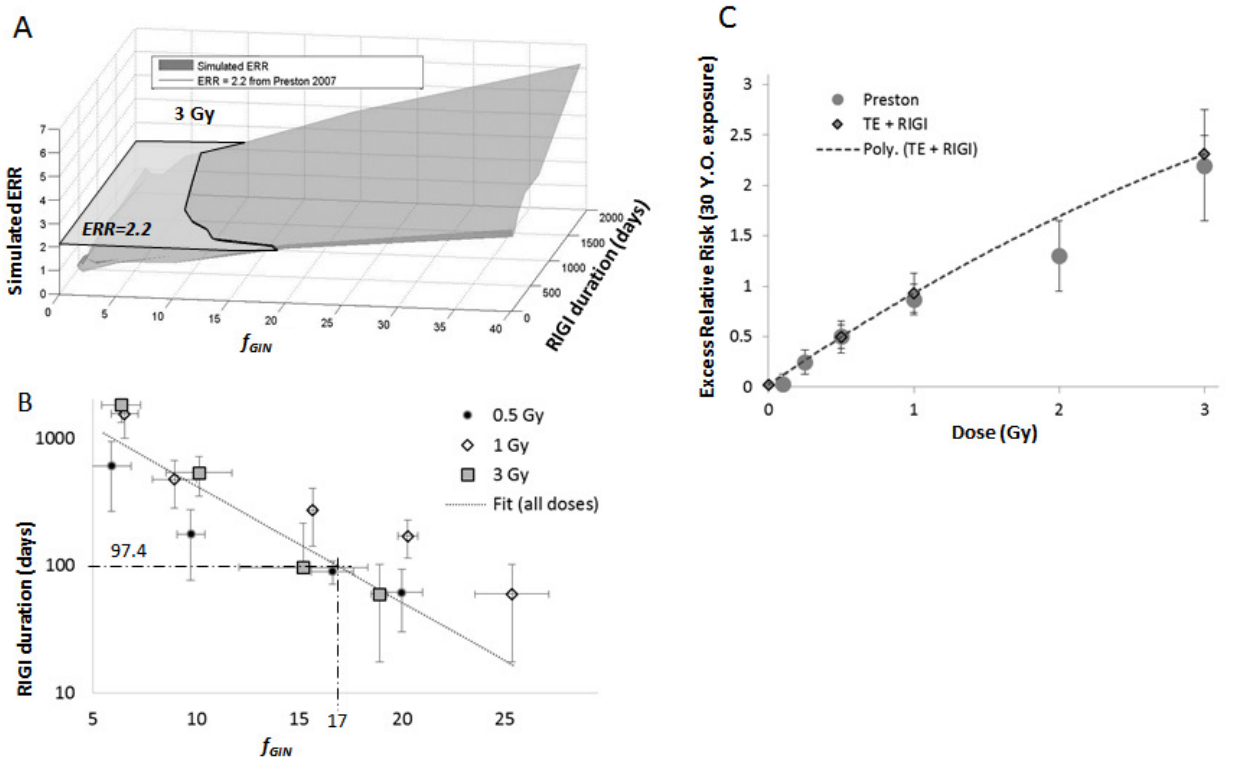

Fig 4B shows the resulting iso-ERR curves generated this way for three doses: 0.5, 1 and 3 Gy. One can note that RIGI duration decreases exponentially with the multiplicative factor f_{GIN} for all three doses simulated. The iso-ERR curves for all three doses are closest when f_{GIN}~17 and RIGI duration is ~97 days (dashed lines in Fig. 4B). Using these parameters, a new set of simulations predicting Preston ERR can be computed (TE+RIGI scenario - Fig. 4C) clearly showing accurate predictions all the way down to 0.2 Gy. Therefore our model confirms that RIGI is dose independent and is triggered by low level ionizing radiation. Note that if we use instead the exponential cell death models (beta X2, beta X3), one cannot find a set of values that can predict the ERR for all doses mainly because it always leads to overestimate for doses larger than 1 Gy (data not shown).

RICI was implemented by increasing the death rate in the entire tissue by a fold increase in a uniform manner for prolonged periods after irradiation. The same approach that was applied for RIGI was done for chronic inflammation (data not shown). Duration of 1825 days and induction fold of 2 were chosen as the best fit. We noted however that The TE + RICI scenario gives less stable results than the TE + RIGI

scenario. This is mainly because there is one more step involved if the chronic inflammation is chosen as non-targeted effect. Indeed, cell mortality is tuned at a higher value, which implies more cell division to fill the gap left by the dead cell. Consequently it also implies more possibility for mutations, not because μ is higher but because there are more daughter cells that can be targeted. In the case of RIGI, only one process is at play: the mutation rate increases, the death rate and the number of targeted cells remain stable. In order to keep less variable outcome in our stochastic model, we chose RIGI as our principal non targeted effect in the rest of this work, allowing to keep the number of simulations reasonable to reach statistical significance.

3.3. Modeling exposure to cosmic radiation

For high LET exposure, the mutation and death rate from Fig. 3 were adjusted to reflect the change of radiation quality using published RBE. The change in death rate was made on the basis of our previous model predicting RBE for 10% survival in MCF10A cells exposed to high LET particles using the principle of DSB clustering as the main factor for higher cell death incidence than for low-LET (7). Even though MCF10A cells are immortalized, they are nonmalignant and they show similar response to primary human breast cells. For example, 10% cell survival of MCF10A is observed after 4 Gy (29) against 4.7 Gy for primary breast cells (43). RBE for mutation rate were based on a study that assessed $HPRT^-$ mutants in mammalian cells after exposure to a range of high LET particles (44). For non-targeted effect, the RIGI scenario was adopted and a RBE of 1 was used as we showed no dose dependence for RIGI in the previous section for low LET. This is in good agreement with our previous work showing in human breast cells that NTE are not increased with high-LET (43).

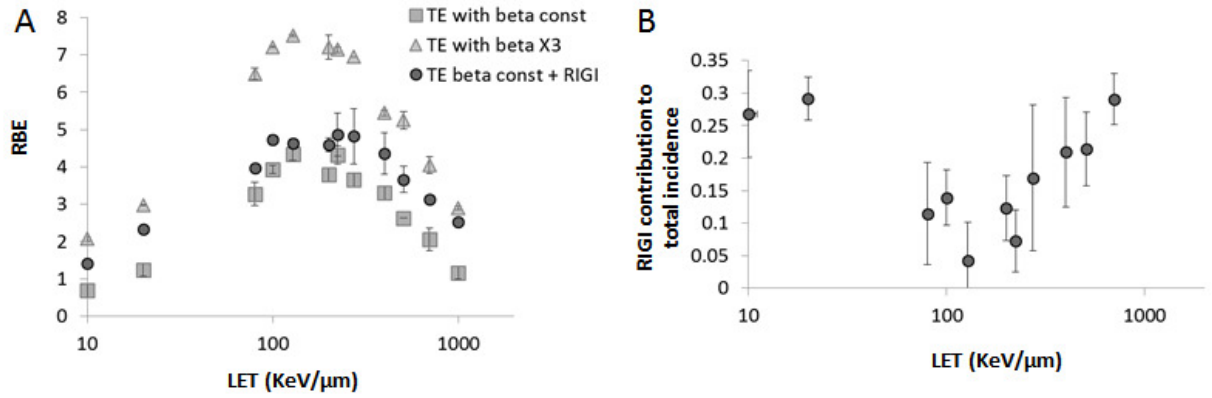

Fig 5A shows RBE prediction for breast cancer induction at age 70 after exposure to 1 Gy of high-LET particles ranging from 10 to 1000 keV/µm with age of exposure at 30 y.o, the low-LET cancer incidence dose dependence to compute the equivalent ERR (Fig 4C). The maximum RBE for breast cancer induction peaks around 220 keV/µm with a value close to 5. For comparison, we used a mutational RBE peaking at 100 keV/µm (44) while survival fraction RBE for breast cells peaks around 400 keV/µm using our previous model (7). This illustrates the relative contribution of both mutational and death events, leading to a competition between RBE peaks. For comparison, we also computed RBE when we only have TE with the exponential cell death model (TE with beta X3) as this led to accurate low-LET ERR for high doses only. As expected, this led to much higher RBE. Finally, in order to better characterize the contribution of RIGI in RBE, we computed the scenario involving only targeted effects with beta constant. One can note in Fig. 5A that the addition of RIGI at low and very high LET leads to a 2-fold increase in RBE for breast cancer induction compared to TE alone (TE with beta const). Another way to visualize the contribution of RIGI is to compute for each simulated LET the additional number of cancers generated in the TE+RIGI scenario against TE only (using beta const in both case). This is shown in Fig. 5B suggesting that nearly 30% of the excess cancers are due to RIGI at low and very high LET, while only 10% at intermediate LET. This is expected as RIGI is dose and LET independent, therefore when TE is maximum (i.e. intermediate LET), RIGI has the lowest contribution. All radiation parameters are summarized in Table 2.

4. Discussion

Modeling the complexity of the tissue response to ionizing radiation has been challenging because of the heterogeneity of tissue, the large time scale between exposure time and cancer detection, and the lack of experimental data needed to inform computer model. As such, deterministic models have been dominating the field (8, 10-13) with epidemiologic data from the A-bomb survivors remaining the gold standard for risk assessment (4). However, the growing complexity of data from radiation biology being unraveled over the past 20 years needs to be taken into account into outdated models and novel approaches bypassing the limitation of epidemiologic approaches have become a necessity for better risk management.

The old paradigm that biological consequences from exposure to radiation arise solely from events occurring at the time of exposure has been challenged in the last two decades by the observation of non-targeted effects (NTE) such as genomic instability, bystander and non-clonal effects, abscopal effect and delayed cell death (45, 46). All have in common that they are displaced in time or space from the initial insult and arise as a consequence of intercellular signaling. The argument has been made that irradiation is not only the initiating lesion but also promotes the acquisition of secondary genetic changes due to NTE, possibly involving long term tissue responses to radiation due to oxidative stress and cytokine production (47). In this work, we chose to concentrate on genomic instability and chronic inflammation for NTE, as they are readily applicable to the cell level used in our *in silico* tissue. Generally there is a lack of evidence for a conventional dose-response relationship for radiation-induced genomic instability (RIGI) with no increased expression at high doses and RIGI is modulated by cell type and genetic predisposition (48).

Persistent subclinical inflammation has been reported in Japanese A-bomb survivors (49). In a chronic inflammation context, production of reactive oxygen/nitrogen species by macrophages or neutrophils causes collateral damage in adjacent cells in the form of mutational events. It is thought that this chronic inflammation may confer predisposition to malignancies and has recently been linked to the development of radiation-induced leukemia (42). In addition, phagocytic uptake of apoptotic cells can result in further apoptosis by the release of soluble signals triggering Fas-mediated apoptosis in bystander cells (50). Another study correlated delayed apoptosis with the appearance of neoplastically transformed *foci* (51).

Over the years our group has developed approaches that distinguish themselves from the classic deterministic models. Our work has benefited from the usage of agent-based models (ABM), a stochastic approach simulating life and emerging properties of complex interacting entities (5, 7, 22). These modeling approaches are well suited for modeling NTE as they allow us to simulate and modify on the fly information related to spatial structure of a tissue, cell heterogeneity, large time scale and cell signaling. Our ABM models have already spanned from disruption of stem cell self-renewal signaling to three-dimensional breast epithelium reorganization and human breast senescence (6, 22). Others have also shown the efficiency of such approaches in modeling the radiation response (52, 53).

In the work presented here, we introduce a simplified agent-based model where a cell is a pixel which cannot move nor interact, but can die or divide to neighboring pixels. We refer to this model as an automaton. Removing the need for tracking individual agents allow us to gain computing speed and to lower memory usage for simulations. This was necessary to produce large *in-silico* cohorts of women exposed to a variety of radiation doses and radiation qualities in an attempt to predict cancer risk from exposure to cosmic radiation. We first implemented the two-stage clonal expansion (TSCE) model with automata to simulate tumor incidence arising spontaneously in human population due to random

mutations. As we have done in previous models (22), breast ducts cut along their length can be modeled as simple 2D sheet of one single cell layer. We also assume that initiated cells are still contact-inhibited and are still attached to the basement membrane and thus remain within the 2D sheet just like normal cells (6). On the other hand, proliferation potential and genomic instability is increased in initiated cells in our model. For TSCE, once an initiated cell acquires another set of gene mutations specific to transformation (mutation rate μ_2), it is classified as a neoplastic cell and its interaction with the basement membrane is compromised allowing it to proliferate inside the lumen (54). Lumen invasion has been modeled in sophisticated 3D *in silico* approaches (6, 55, 56) but these later models require large computer frameworks when handling millions of cells and millions of simulations. In order to keep size and simulation time manageable, we therefore kept the model as a 2D sheet where neoplastic cells invade neighboring cells instead of growing within the lumen in the case of 3D models. We found that detection time was a function of invasion parameters and detectable size programmed within the model and modifying these parameters only change the lag-time not the cancer frequencies. Therefore, using a 3D model would not have changed our conclusions.

After identifying parameters leading to accurate spontaneous rate observed in the female population for breast cancer, we modeled an acute radiation exposure by modifying these parameters based on experimental data. We first modeled targeted effects (TE) by modifying mutation rates and cell death rates for a short duration after an acute exposure (1 and 14 days respectively). Perturbations of the TSCE model led to higher cancer incidence, allowing us to compute an excess relative risk (ERR) for various doses of low-LET. The predicted ERR were lower than A-bomb breast cancer ERR for doses lower than 2 Gy, suggesting TE alone cannot fully explain radiation-induced carcinogenesis and that NTE are also contributing. The NTE model that best explained the A-bomb data was the induction of a chronic level of genomic instability ~17 times higher than spontaneous levels lasting 97 days following exposure to low-LET. Induction of genomic instability was dose independent and thus added for all simulated doses

(>0.1Gy). On the other hand, the model could not let us conclude definitely on the absolute duration and intensity of radiation induced genomic instability (RIGI). For instance, a shorter duration could lead to the same outcome if genomic instability was set higher. To put this result into perspective let us compare the model to experimental observations. For in vitro data, it was shown that RIGI presents the same kind of mutation spectrum than spontaneous mutations and can persist over many cell doublings: i.e. more than 40 divisions in mammary epithelial cells exposed to γ-rays or neutrons (57). Similarly, *In vivo* experiments involving mice have reported RIGI lasting up to one year after irradiation (58).

Kaiser et al have also looked at the relative contribution of TE and NTE to fit the A-bomb ERR at 1 Gy using empirical models mixed with a deterministic implementation of TSCE (59). In their model, they concluded that the age dependence of ERR could be explained by three different modes of actions for radiation: either direct effect on initiation alone; long-life increase of proliferation of pre-cancerous cells; or long-life increase of genomic instability. In their model however, there are no biological parameters derived from experiments and the model does not represent spatial constraints from a tissue in homeostasis. In our case, we directly visualize the impact of various biological mechanisms on carcinogenesis, giving us more biological insights than simply fitting a curve.

Once the NTE model was established for low-LET, we challenged our model to predict breast cancer incidence in an artificial human cohort exposed to various high-LET particles. This was done by simply modifying the TE parameters using published RBE for cell death and mutation. In turn, we predicted RBE for breast cancer induction, which reached a maximum of 5 following 220 keV/µm. In contrast, RBE were close to 1 for LET>1000 keV/µm or LET<10 keV/µm. Note that the LET-dependence used for cell death RBE is based on the concept that DNA double strand breaks (DSB) are naturally gathered into common repair center (36, 60), a paradigm that leads to higher cell death at high dose or higher LET in human breast epithelial cells (7). One could have used published RBE on other cell lines (61) instead of

these theoretical RBEs. Using published RBE instead would still lead to similar cancer RBE since values and dose curve looked very similar. The advantage of using theoretical death RBE based on DSB clustering formalism (7) is the fact that we can predict any dose, dose rate and LET scenarii.

In order to put these RBE predictions into perspective, we should compare them to the most comprehensive dataset for tumor induction after high LET irradiation (2, 62). LET ranging from ~1.5 to 170 keV/µm were investigated in mice and RBE values for Harderian gland tumor incidence were measured to be much higher than our models with RBE ~27-40 for ^{56}Fe. The Harderian gland is not an organ present in humans, and these RBE discrepancies illustrate the ongoing challenge of scaling data from mice to humans. However, one potential explanation is the fact that NTE may account for some of these discrepancies reflecting the very distinct microenvironment of tissues and species. In particular, Cucinotta et al. derived an analytical model to fit the Harderian gland tumor prevalence and showed that NTE had a significant impact by increasing RBE for very low and very high LET (63). This result is in agreement with our model where NTE is triggered for any simulated doses in an equal manner, making it relatively more significant also at extreme LET or at low doses (Figs. 4C and 5).

5. Conclusion

At present, our automata model can provide RBE for breast cancer induction with a large panel of particle radiations. Other types of cancers can be implemented in a few steps. First, the calibration for spontaneous cancer induction has to be performed and spontaneous mutation and death rates will be obtained for a specific tissue. Next, the death rate following irradiation has to be adapted. This is easily done on the basis of survival fraction for a specific cell line exposed to X-rays and using our previous formalism on DSB clustering to predict death rate for high-LET radiation (7). However, a knowledge gap exists regarding RIGI with many remaining questions: Is there a dose threshold for RIGI? What is the

dependence of RIGI with respect to species and tissues? Is there any dose shape curve for RIGI past the threshold? How does RIGI change in the context of chronic exposure?

Finally, in the context of space missions, in particular incoming missions to Mars where astronauts are expected to be exposed to more than 1 Sv in the course of a three year mission, risks are currently poorly determined. Space conditions of chronic low doses of high LET have been an ongoing challenge for modeling long-term health hazard from space radiation. It may become a reality with our model, as it provides a tool to simulate real space conditions with both LET and time scales being fully compatible for chronic exposure over days or months. We believe in the future that physiological information obtained on Astronauts before, during and after a mission could be integrated into our model to better inform long-term effects such as NTE and RIGI and create more accurate risk models.

Acknowledgments

We wanted to thank Dr. Louise Viger for her constructive feedback on the manuscript. ACH is a postdoctoral fellow supported by the Belgian American Education Foundation, the Fulbright Commission and the Walloon region of Belgium (WBI). SVC, JT and AO are supported by NASA fundings [NNL15AA08I].

Table 1 Summary of Input parameters leading to accurate spontaneous breast cancer incidence.

Input parameters	**Value (day^{-1})**
Baseline	
Death rate β_1 (stage 1 – hormonally driven) average at 20 y.o. (See Fig. 2A for all values)	1.8 e-3
Death rate β_2 (stage 2 – age independent)	3.1 e-3
Death rate β_3 (stage 3 – age independent)	5.6 e-3
Mutation rate μ_n (stage n → stage n+1)	n x 3.8 e-6
Senescence factor	5 e-9

Tumor growth	1/365

Table 2 Radiation parameters

Targeted effects	
Low-LET	
Radiation μ $\mu(D) = 60.\mu.D$	Multiplicative factor proportional to dose
Radiation β survival = exp(-0.084.D^2 - 0.273.D)	Dose-dependent additive factor from clonogenic survival data from Lin et al. (29)
High-LET	RBE for μ (44) and for β (7)
Non targeted effects (LET and dose independent)	
RIGI μ	17 multiplicative factor
RIGI duration	97 days
Inflammation β	2 multiplicative factor
Inflammation duration	1825 days

References

1. Cucinotta FA, Durante M. Cancer risk from exposure to galactic cosmic rays: implications for space exploration by human beings. The Lancet Oncology. 2006;7(5):431-5.
2. Alpen EL, Powers-Risius P, Curtis SB, DeGuzman R. Tumorigenic potential of high-Z, high-LET charged-particle radiations. Radiat Res. 1993;136(3):382-91.
3. Chancellor JC, Scott GB, Sutton JP. Space Radiation: The Number One Risk to Astronaut Health beyond Low Earth Orbit. Life (Basel). 2014;4(3):491-510.
4. Preston DL, Ron E, Tokuoka S, Funamoto S, Nishi N, Soda M, et al. Solid cancer incidence in atomic bomb survivors: 1958-1998. Radiat Res. 2007;168(1):1-64.
5. Mukhopadhyay R, Costes SV, Bazaro A, Hines WC, Barcellos-Hoff MH, Yaswen P. Promotion of variant human mammary epithelial cell outgrowth by ionizing radiation: an agent-based model supported by in vitro studies In Press. 2010.
6. Tang J, Enderling H, Becker-Weimann S, Pham C, Polyzos A, Chen CY, et al. Phenotypic transition maps of 3D breast acini obtained by imaging-guided agent-based modeling. Integrative biology : quantitative biosciences from nano to macro. 2011;3(4):408-21.
7. Vadhavkar N, Pham C, Georgescu W, Deschamps T, Heuskin AC, Tang J, et al. Combinatorial DNA Damage Pairing Model Based on X-Ray-Induced Foci Predicts the Dose and LET Dependence of Cell Death in Human Breast Cells. Radiat Res. 2014.
8. Ritter G, Wilson R, Pompei F, Burmistrov D. The multistage model of cancer development: some implications. Toxicology and industrial health. 2003;19(7-10):125-45.
9. Armitage P. Multistage models of carcinogenesis. Environmental health perspectives. 1985;63:195-201.
10. Hayflick L. The Limited in Vitro Lifetime of Human Diploid Cell Strains. Exp Cell Res. 1965;37:614-36.
11. Pompei F, Polkanov M, Wilson R. Age distribution of cancer in mice: the incidence turnover at old age. Toxicology and industrial health. 2001;17(1):7-16.
12. Heidenreich WF, Luebeck EG, Hazelton WD, Paretzke HG, Moolgavkar SH. Multistage models and the incidence of cancer in the cohort of atomic bomb survivors. Radiat Res. 2002;158(5):607-14.
13. Heidenreich WF, Luebeck EG, Moolgavkar SH. Some properties of the hazard function of the two-mutation clonal expansion model. Risk Anal. 1997;17(3):391-9.
14. Anderson TJ, Ferguson DJ, Raab GM. Cell turnover in the "resting" human breast: influence of parity, contraceptive pill, age and laterality. Br J Cancer. 1982;46(3):376-82.
15. Potten CS, Watson RJ, Williams GT, Tickle S, Roberts SA, Harris M, et al. The effect of age and menstrual cycle upon proliferative activity of the normal human breast. Br J Cancer. 1988;58(2):163-70.
16. Navarrete MA, Maier CM, Falzoni R, Quadros LG, Lima GR, Baracat EC, et al. Assessment of the proliferative, apoptotic and cellular renovation indices of the human mammary epithelium during the follicular and luteal phases of the menstrual cycle. Breast cancer research : BCR. 2005;7(3):R306-13.
17. Li JJ, Li SA, Daling JR. Hormonal Carcinogenesis III: Springer Science & Business Media; 2001.
18. Greer W, Sandridge AL, Chehabeddine RS. The frequency distribution of age at natural menopause among Saudi Arabian women. Maturitas. 2003;46(4):263-72.
19. Herbig U, Ferreira M, Condel L, Carey D, Sedivy JM. Cellular senescence in aging primates. Science. 2006;311(5765):1257.
20. Campisi J, d'Adda di Fagagna F. Cellular senescence: when bad things happen to good cells. Nature reviews Molecular cell biology. 2007;8(9):729-40.
21. N H, AM N, M K, J G, D M, SF A, et al. SEER Cancer Statistics Review, 1975-2012, National Cancer Institute. Bethesda, MD. http://seer.cancer.gov/csr/1975_2012/2015.

519 22. Tang J, Fernandez-Garcia I, Vijayakumar S, Martinez-Ruiz H, Illa-Bochaca I, Nguyen DH, et al.
520 Irradiation of juvenile, but not adult, mammary gland increases stem cell self-renewal and estrogen
521 receptor negative tumors. Stem cells. 2013.
522 23. Parton M, Dowsett M, Smith I. Studies of apoptosis in breast cancer. Bmj. 2001;322(7301):1528-
523 32.
524 24. Gandhi A, Holland PA, Knox WF, Potten CS, Bundred NJ. Evidence of significant apoptosis in
525 poorly differentiated ductal carcinoma in situ of the breast. Br J Cancer. 1998;78(6):788-94.
526 25. Zhao H, Morimoto T, Sasa M, Tanaka T, Izumi K. Immunohistochemical expression of uPA, PAI-1,
527 cathepsin D and apoptotic cells in ductal carcinoma in situ of the breast. Breast cancer. 2002;9(2):118-
528 26.
529 26. Campisi J. Aging, cellular senescence, and cancer. Annual review of physiology. 2013;75:685-
530 705.
531 27. Rodier F, Campisi J. Four faces of cellular senescence. J Cell Biol. 2011;192(4):547-56.
532 28. Campisi J, Sedivy J. How does proliferative homeostasis change with age? What causes it and
533 how does it contribute to aging? The journals of gerontology Series A, Biological sciences and medical
534 sciences. 2009;64(2):164-6.
535 29. Lin YF, Nagasawa H, Peng Y, Chuang EY, Bedford JS. Comparison of several radiation effects in
536 human MCF10A mammary epithelial cells cultured as 2D monolayers or 3D acinar stuctures in matrigel.
537 Radiat Res. 2009;171(6):708-15.
538 30. Wera AC, Heuskin AC, Riquier H, Michiels C, Lucas S. Low-LET proton irradiation of A549 non-
539 small cell lung adenocarcinoma cells: dose response and RBE determination. Radiat Res.
540 2013;179(3):273-81.
541 31. Sakashita T, Hamada N, Kawaguchi I, Ouchi NB, Hara T, Kobayashi Y, et al. A framework for
542 analysis of abortive colony size distributions using a model of branching processes in irradiated normal
543 human fibroblasts. PLoS One. 2013;8(7):e70291.
544 32. Sakashita T, Hamada N, Kawaguchi I, Hara T, Kobayashi Y, Saito K. A branching process model for
545 the analysis of abortive colony size distributions in carbon ion-irradiated normal human fibroblasts.
546 Journal of radiation research. 2014;55(3):423-31.
547 33. Sachs RK, Brenner DJ, Chen AM, Hahnfeldt P, Hlatky LR. Intra-arm and interarm chromosome
548 intrachanges: tools for probing the geometry and dynamics of chromatin. Radiat Res. 1997;148(4):330-
549 40.
550 34. Wu H, Sachs RK, Yang TC. Radiation-induced total-deletion mutations in the human hprt gene: a
551 biophysical model based on random walk interphase chromatin geometry. Int J Radiat Biol.
552 1998;73(2):149-56.
553 35. Costes S, Sachs R, Hlatky L, Vannais D, Waldren C, Fouladi B. Large-mutation spectra induced at
554 hemizygous loci by low-LET radiation: evidence for intrachromosomal proximity effects. Radiat Res.
555 2001;156(5 Pt 1):545-57.
556 36. Costes SV, Ponomarev A, Chen JL, Nguyen D, Cucinotta FA, Barcellos-Hoff MH. Image-based
557 modeling reveals dynamic redistribution of DNA damage into nuclear sub-domains. PLoS Comput Biol.
558 2007;3(8):e155.
559 37. Chiolo I, Minoda A, Colmenares SU, Polyzos A, Costes SV, Karpen GH. Double-strand breaks in
560 heterochromatin move outside of a dynamic HP1a domain to complete recombinational repair. Cell.
561 2011;144(5):732-44.
562 38. Denoyer D, Lobachevsky P, Jackson P, Thompson M, Martin OA, Hicks RJ. Analysis of 177Lu-
563 DOTA-octreotate therapy-induced DNA damage in peripheral blood lymphocytes of patients with
564 neuroendocrine tumors. J Nucl Med. 2015;56(4):505-11.
565 39. Djuzenova CS, Elsner I, Katzer A, Worschech E, Distel LV, Flentje M, et al. Radiosensitivity in
566 breast cancer assessed by the histone gamma-H2AX and 53BP1 foci. Radiation oncology. 2013;8:98.

40. Mumbrekar KD, Fernandes DJ, Goutham HV, Sharan K, Vadhiraja BM, Satyamoorthy K, et al. Influence of double-strand break repair on radiation therapy-induced acute skin reactions in breast cancer patients. Int J Radiat Oncol Biol Phys. 2014;88(3):671-6.
41. Tang j, Georgescu W, Deschamps T, Yannone SM, Costes SV. Mathematical Modeling for DNA Repair, Carcinogenesis and Cancer Detection. Genomic Instability and Cancer Metastasis: Springer Science & Business Media; 2015. p. 75–93.
42. Joiner M, Kogel Avd. Basic clinical radiobiology. 4th ed. London: Hodder Arnold ;; 2009. vi, 375 p. p.
43. Andarawewa KL, Costes SV, Fernandez-Garcia I, Chou WS, Ravani SA, Park H, et al. Lack of radiation dose or quality dependence of epithelial-to-mesenchymal transition (EMT) mediated by transforming growth factor beta. Int J Radiat Oncol Biol Phys. 2011;79(5):1523-31.
44. Kiefer J, Schmidt P, Koch S. Mutations in mammalian cells induced by heavy charged particles: an indicator for risk assessment in space. Radiat Res. 2001;156(5 Pt 2):607-11.
45. Lorimore SA, Coates PJ, Wright EG. Radiation-induced genomic instability and bystander effects: inter-related nontargeted effects of exposure to ionizing radiation. Oncogene. 2003;22(45):7058-69.
46. Wright EG, Coates PJ. Untargeted effects of ionizing radiation: implications for radiation pathology. Mutat Res. 2006;597(1-2):119-32.
47. Mukherjee D, Coates PJ, Lorimore SA, Wright EG. Responses to ionizing radiation mediated by inflammatory mechanisms. The Journal of pathology. 2014;232(3):289-99.
48. Wright EG. Inducible genomic instability: new insights into the biological effects of ionizing radiation. Medicine, conflict, and survival. 2000;16(1):117-30; discussion 31-3.
49. Neriishi K, Nakashima E, Delongchamp RR. Persistent subclinical inflammation among A-bomb survivors. Int J Radiat Biol. 2001;77(4):475-82.
50. Brown SB, Savill J. Phagocytosis triggers macrophage release of Fas ligand and induces apoptosis of bystander leukocytes. Journal of immunology. 1999;162(1):480-5.
51. Mendonca MS, Howard KL, Farrington DL, Desmond LA, Temples TM, Mayhugh BM, et al. Delayed apoptotic responses associated with radiation-induced neoplastic transformation of human hybrid cells. Cancer Res. 1999;59(16):3972-9.
52. Enderling H, Park D, Hlatky L, Hahnfeldt P. The Importance of Spatial Distribution of Stemness and Proliferation State in Determining Tumor Radioresponse. Math Model Nat Pheno. 2009;4(3):117-33.
53. Gao X, McDonald JT, Hlatky L, Enderling H. Acute and fractionated irradiation differentially modulate glioma stem cell division kinetics. Cancer Res. 2013;73(5):1481-90.
54. Bissell MJ, Rizki A, Mian IS. Tissue architecture: the ultimate regulator of breast epithelial function. Current opinion in cell biology. 2003;15(6):753-62.
55. Gatenby RA, Gillies RJ. Why do cancers have high aerobic glycolysis? Nat Rev Cancer. 2004;4(11):891-9.
56. Macklin P, Edgerton ME, Thompson AM, Cristini V. Patient-calibrated agent-based modelling of ductal carcinoma in situ (DCIS): from microscopic measurements to macroscopic predictions of clinical progression. J Theor Biol. 2012;301:122-40.
57. Ponnaiya B, Cornforth MN, Ullrich RL. Induction of chromosomal instability in human mammary cells by neutrons and gamma rays. Radiat Res. 1997;147(3):288-94.
58. Watson GE, Lorimore SA, Wright EG. Long-term in vivo transmission of alpha-particle-induced chromosomal instability in murine haemopoietic cells. Int J Radiat Biol. 1996;69(2):175-82.
59. Kaiser JC, Jacob P, Meckbach R, Cullings HM. Breast cancer risk in atomic bomb survivors from multi-model inference with incidence data 1958-1998. Radiation and environmental biophysics. 2012;51(1):1-14.

60. Neumaier T, Swenson J, Pham C, Polyzos A, Lo AT, Yang P, et al. Evidence for formation of DNA repair centers and dose-response nonlinearity in human cells. Proc Natl Acad Sci U S A. 2012;109(2):443-8.
61. Lett JT, Cox AB, Story MD, Ehmann UK, Blakely EA. Responses of synchronous L5178Y S/S cells to heavy ions and their significance for radiobiological theory. Proc R Soc Lond B Biol Sci. 1989;237(1286):27-42.
62. Fry RJ, Powers-Risius P, Alpen EL, Ainsworth EJ, Ullrich RL. High-LET radiation carcinogenesis. Adv Space Res. 1983;3(8):241-8.
63. Cucinotta FA, Chappell LJ. Non-targeted effects and the dose response for heavy ion tumor induction. Mutat Res. 2010;687(1-2):49-53.

Figure legends

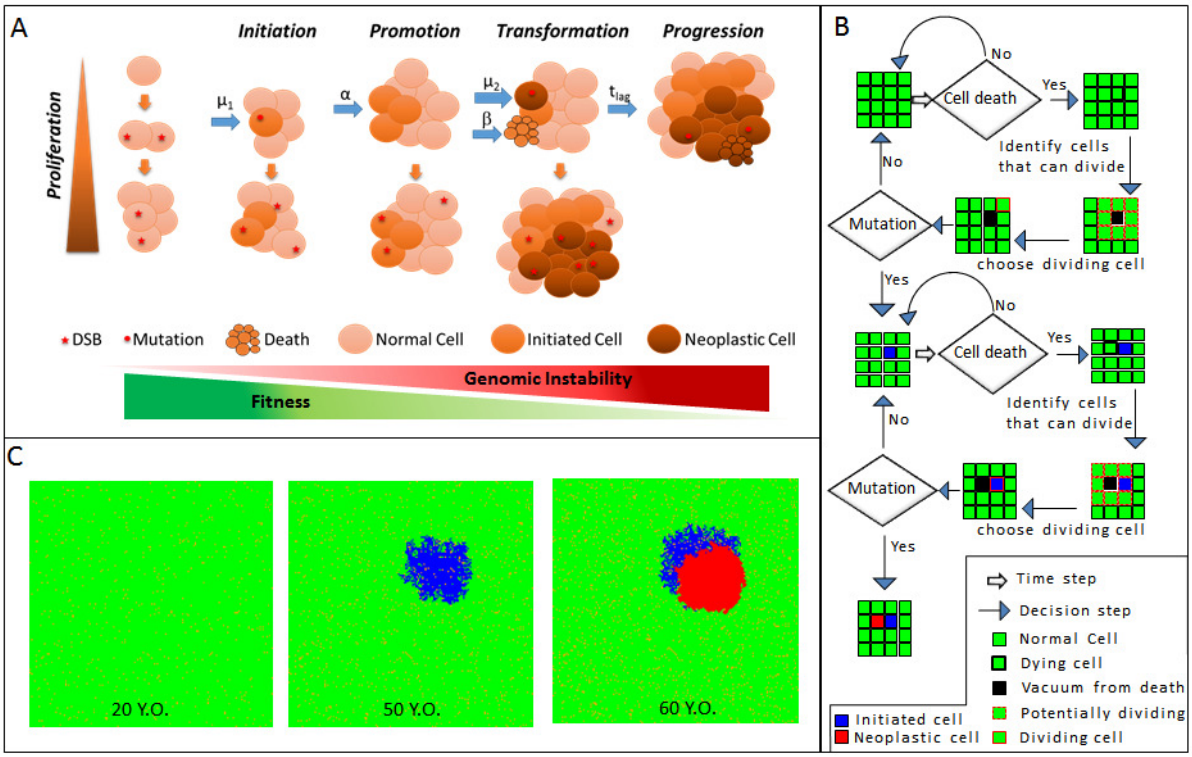

Fig 1. Sketch of the automata carcinogenesis model. (A) Illustration of TSCE, with μ_1 and μ_2 which represent the mutation rates for initiated and malignant cells respectively. α is the turnover rate whereas β is the death rate. t_{lag} is the necessary time for a detectable tumor to form. (B) Flow chart of automata illustrating how a pixel can become a tumor cell. (C) Snapshot of one simulation leading to a tumor: (Green) Normal cell, (Blue) Initiated cell, (Red) Malignant cell, (Orange) Senescent cell.

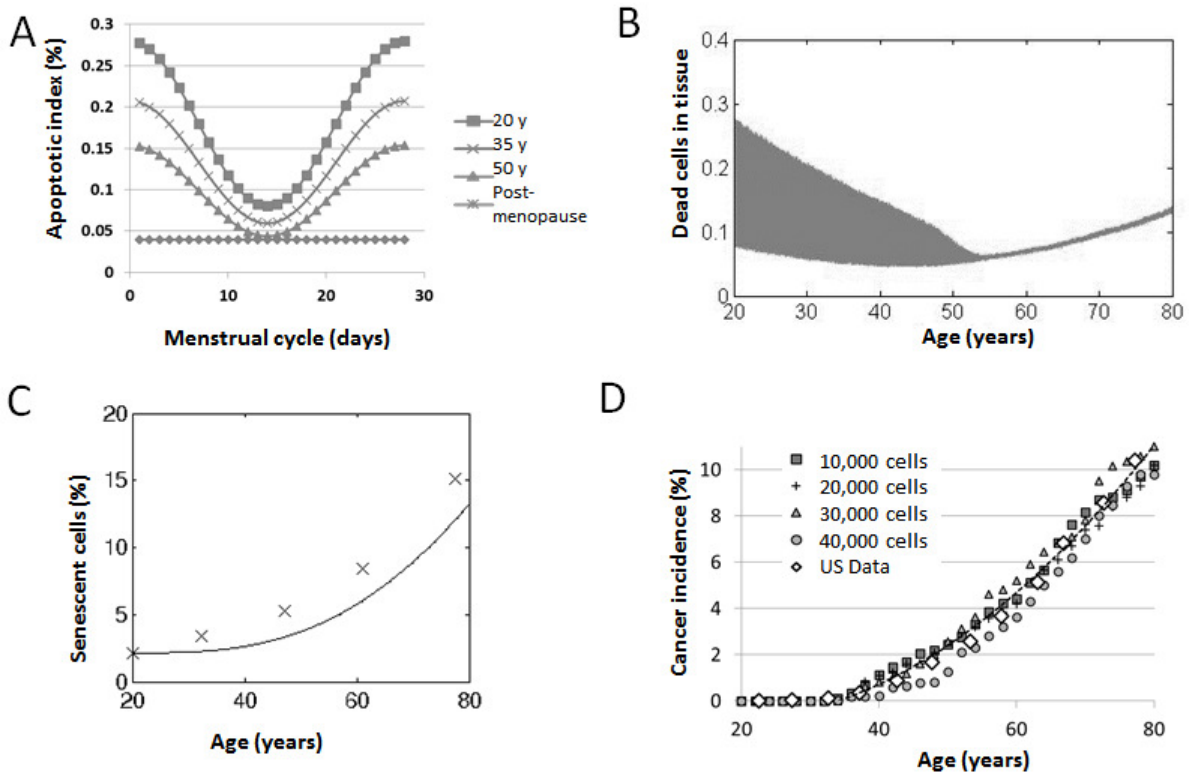

631

632 **Fig 2. Model calibration on spontaneous breast cancer incidence.** (A) The death rate β is set periodic to
633 match the menstrual cycle, with an amplitude and baseline that decreases with age until reaching
634 menopause where rate stabilizes at 0.4e-3 per day. (B) Average number of dying cells as tissue ages *in*
635 *silico*. (C) Simulation of the percentage of senescent cells in the tissue compared to published data for
636 primate (19). Best fit is obtained for a senescence factor = 5e-9 and was set as a fixed parameter. (D)
637 Average simulations of 500 tissues *in silico* predicting cumulated incidence of breast cancer at a given
638 age (21). Calibration parameters that led to the lowest mean error square between predicted cancer
639 incidence and epidemiological data for the US are given in Table 1. Calibration of mutation rate was
640 done for various initial tissue sizes (i.e. 100x100, 200x100, 200x150, 200x200), showing large initial
641 tissue leads to lower mutation rate.

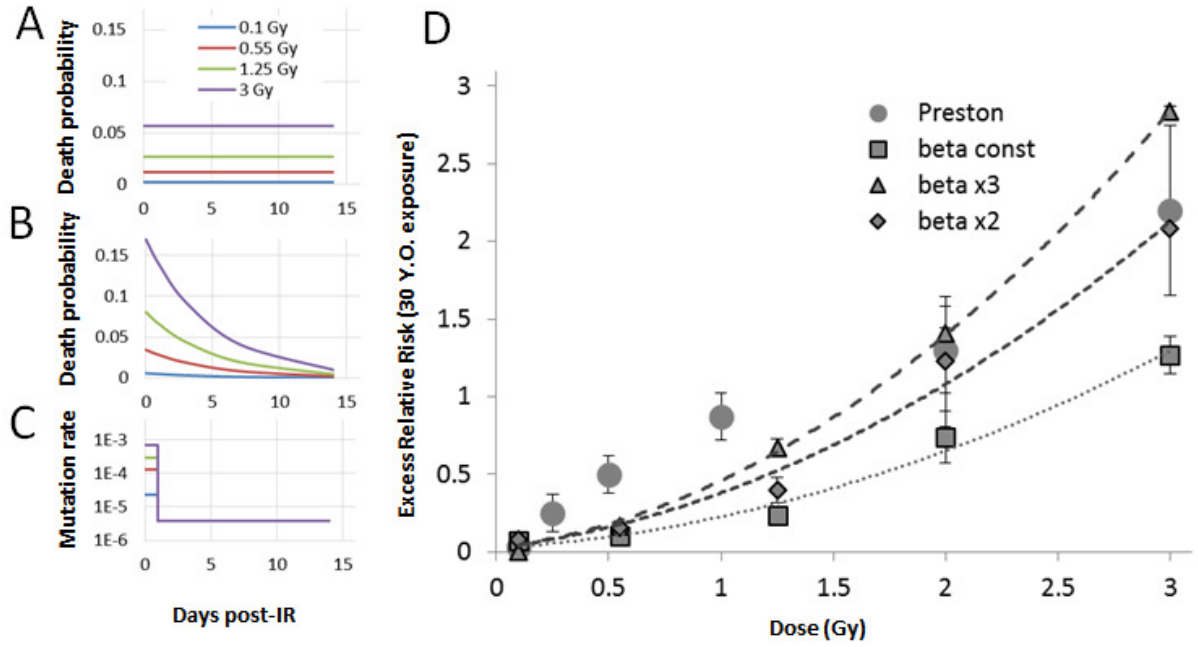

642
643 **Fig 3. Model calibration for low LET induced breast cancer incidence.** (A) Death levels are set based on
644 clonogenic data but with death spread evenly over a 14 day period (30). (B) Second death model,
645 assuming the same overall level of death but with death spread following an exponential decay over 14
646 day period (31, 32). In this example, initial death at day 0 is 3 times larger than in the constant model in
647 (A). We also considered 2 fold differences. (C) Mutation rates are assumed to be increased only for one
648 day after exposure to ionizing radiation. For simplification rate of mutation is set proportional to the
649 baseline rate found for spontaneous damage based on experimental data using a linear dependence
650 with dose (see Material and Method). Legend shows some of the tested doses in Gy. (D) Predicted
651 excess relative risk dose dependence of breast cancer at age 70 assuming exposure at age 30. Each solid
652 line represents a set of 500 simulated in silico women, exposed at a given age using TE only scenario.
653 Simulations for various cell death models are compared to A-bomb data (4) (plotted as full circles for age
654 of exposure equals to 30 y.o.).

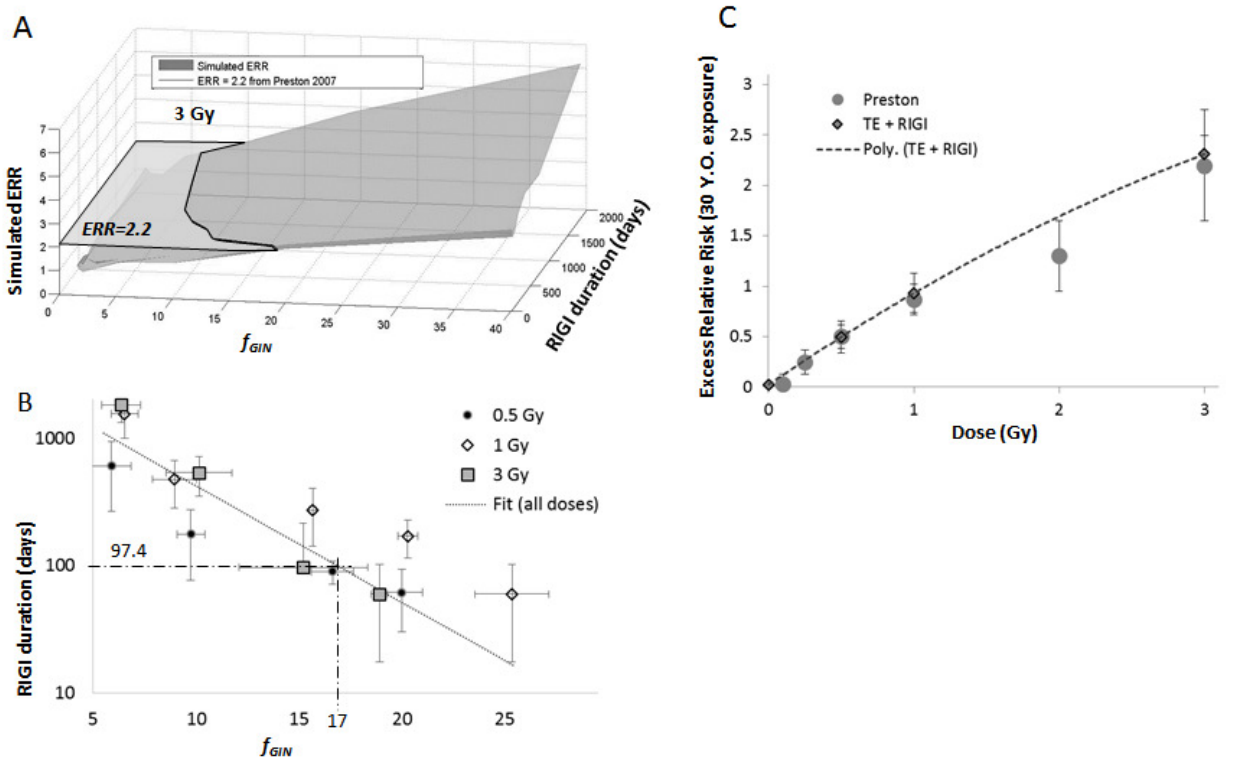

Fig 4. Simulated ERR at age 70 using TE + RIGI scenario as a function of mutation rate and duration. (A) Simulations for 3 Gy exposure at age 30. Experimental ERR (4) is shown intersecting predicted ERR, allowing to define a set of mutation rate and duration that lead to accurate ERR. (B) RIGI duration and mutation rates giving the right ERR for irradiation with 0.5, 1 or 3 Gy X-rays. Dashed line shows the point couple chosen for subsequent simulations (induction fold of 17 over 97 days) (C) Predicted excess relative risk dose dependence of breast cancer at age 70 assuming exposure at age 30 using TE+RIGI scenario.

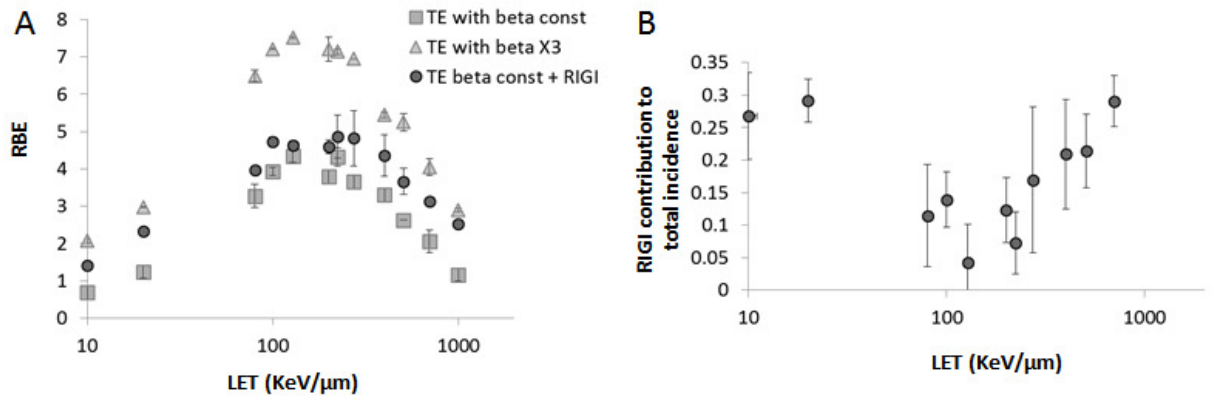

Fig 5. Predicting high-LET RBE. (A) RBE for breast cancer induction following irradiation with 1 Gy of charged particles of various LET. (Circles) Targeted effect (beta const) + radiation induced genomic instability scenario; (Squares) Targeted effect alone (beta const); (Triangles) Targeted effect alone using exponential decay model for radiation-induced cell death (B) Fractional contribution of non-targeted effects to breast cancer induction after irradiation with charged particles of various LET.